MODEL-BASED ANALYSIS AND INTERPRETATION OF HUMAN EPICARDIAL ELECTROGRAMS USING A BIDOMAIN SLAB MODEL

L. Fritz*, A.J. Prassl**, H. Hutten* and G. Plank**

* Institute of Medical Engineering, Graz University of Technology, Graz, Austria
** Institute of Biophysics, Medical University of Graz, Graz, Austria

L.Fritz@gmx.at

Abstract: A three dimensional bidomain slab model was developed to examine the effects of different conductivity settings, fiber rotation and transmural action potential (AP) heterogeneity on excitation spreading and the subsequent repolarization. Extracellular currents were injected at sites near the epicardial surface to induce different activation sequences. AP propagation was simulated for an entire AP cycle. As expected, the shape of the depolarization wavefront, represented by the transmembrane current, I_m, mainly depends on conductivity settings and fiber orientation which is associated with a noticeable variation in simulated extracellular potentials, Φ_e. During repolarization, in addition variations of the AP shape influence the Φ_e electrograms. Hence, to understand subtle differences in epicardially recorded electrograms further detailed simulation studies are required which account for complexities present in experimental or clinical settings.

Keywords: cardiac modeling, finite-element method, excitation propagation, repolarization

Introduction

Epicardial electrograms can be recorded and transmitted by pacemakers with telemetric capabilities. These signals are assumed to comprise relevant diagnostic information. Preliminary studies used statistical analysis to interpret deviations in the measured signals for rejection detection of transplanted hearts [1], for assessment of the hemodynamic performance [2] and as a clinical marker for disease induced hemodynamic changes [3].

However the signal morphology of the epicardial electrograms is not completely understood yet. Little is known why experimentally or clinically recorded signals show a wide variation different from the theoretically predicted basic waveform and by which factors these deviations are caused. Therefore in a first step a bidomain slab model was developed to investigate the impact of typical parameter settings and assumptions commonly used for the modelling of cardiac tissue. The bidomain formulation was chosen due to its capability to incorporate both the intra- and extracellular spaces.

Materials and Methods

A wedge preparation of a human left ventricular free wall was approximated by a slab model of size 4 x 4 x 1 cm³. Both epicardium and endocardium were covered by a conductive bath of 1 cm thickness. The myocardial slab was discretized using the finite element method with linear tetrahedral elements of 275 µm average edge length. The bath was modelled using an adaptive mesh with growing segment lengths from 250 µm near the myocardium up to 1.75 mm at the distant surface. Either four stimulation sites (O, L, T, C) with size 1 x 1 x 1 mm³ were chosen in the bath close to the epicardial surface to initiate different activation sequences, or an entire lateral surface was stimulated to initiate a planar wavefront. The upper distant edge of the epicardial bath was grounded. Figure 1 shows the simulation setup.

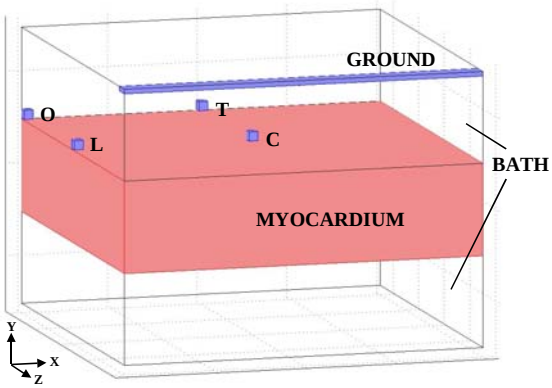

Figure 1: Geometry of the 3D slab covered by the conductive bath. The four stimulation sites are positioned 100 µm above the epicardial border. The ground is placed in the distant epicardial volume conductor.

At the present time the bidomain formulation is the most complete description of cardiac electrical activity. It includes the intracellular potential Φ_i as well as the extracellular potential Φ_e, linking both through the membrane behaviour [4,5]. In this work the decoupled version of the bidomain equations (1), (2) was used. For this representation both systems can be treated independently, and therefore the elliptic problem (1) and the parabolic problem (2) can be solved with different time steps. The elliptic equations were solved using the

ISSN: 1727-1983

conjugate gradient method with an incomplete LU decomposition preconditioner. The parabolic system and the ODEs for the kinetic model were solved using the forward Euler method.

$$\begin{bmatrix} \nabla \cdot (\overline{\sigma}_i + \overline{\sigma}_e) \nabla \Phi_e \\ \nabla \cdot \sigma_{bath} \nabla \Phi_e \end{bmatrix} = \begin{bmatrix} -\nabla \cdot \overline{\sigma}_i \nabla V_m \\ -I_e \end{bmatrix} \quad (1)$$

$$\nabla \cdot \overline{\sigma}_i \nabla V_m = -\nabla \cdot \overline{\sigma}_i \nabla \Phi_e + \beta I_m \quad (2)$$

$\overline{\sigma}_i$ and $\overline{\sigma}_e$ are the conductivity tensors, σ_{bath} the bath conductivity and β (140000 1/m) the surface to volume ratio of the cardiac cells. The transmembrane potential is determined by $V_m = \Phi_i - \Phi_e$. I_e is the applied extracellular current density. The transmembrane current I_m is calculated as:

$$I_m = C_m \frac{\partial V_m}{\partial t} + I_{ion} \quad (3)$$

where C_m (1 µF/cm²) is the transmembrane capacitance and I_{ion} is the ionic current density. Assuming a slower change of Φ_e than V_m the ratio of the applied time steps was 100 µs : 20 µs resulting in a significant reduction of computation time. The only detectable difference to a ratio of 1:1 was the value of Φ_e during stimulation. This may be of importance for defibrillation studies but can be neglected here.

In order to simulate the membrane kinetics the model of Ten Tusscher et al. [6] was used. This model is based on human ventricular data and can reproduce the different AP shapes corresponding to the endocardial, epicardial and midmyocardial regions. This heterogeneity is modelled by differences in the slow rectifier and transient outward currents. Figure 2 shows the AP shapes for the different ventricular regions. The midmyocardial AP duration (APD) is significant longer, and for the endocardial AP the notch after depolarization is almost absent.

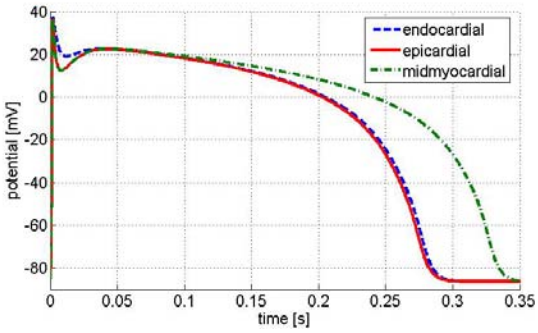

Figure 2: AP shapes of the different ventricular regions for a basic cycle length of 1000 ms.

In our geometry the thickness of the epicardial and endocardial regions was chosen as 2.5 mm, and the thickness of the midmyocardial layer as 5 mm (Figure 3A). For simulations with a uniform AP distribution over the whole myocardial region the epicardial setting was used.

The conductivity tensor was chosen to model either straight parallel fibers (in x direction) with different anisotropy settings or fiber rotation across the ventricular wall. The fiber rotation was modelled by varying the angle of elevation from +70° on the epicardial surface to -60° on the endocardial surface (Figure 3B).

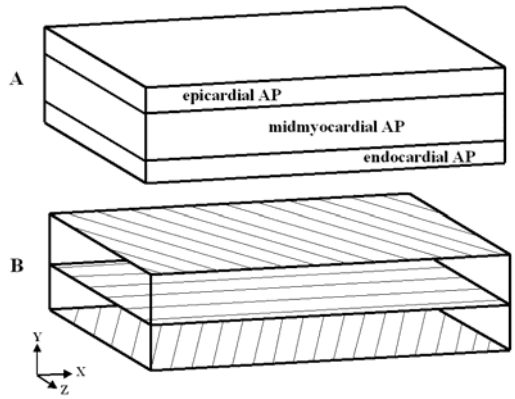

Figure 3: A) Distribution of the transmural AP heterogeneity. B) Schematic of the fiber rotation showing the fiber direction in the epicardium, in the middle of the slab and in the endocardium.

The following cases were considered: 1) isotropic case, 2) equal anisotropy ratios, 3) unequal anisotropy ratios, 4) unequal anisotropy ratios with transmural fiber rotation, 5) same as 3) with transmural heterogeneities of the AP, and 6) same as 4) also with the transmural variation of the AP.

For isotropic setting σ_{i_iso} = 0.077 S/m and σ_{e_iso} = 0.407 S/m were used. In case of unequal anisotropy ratios the intracellular conductivities were set to σ_{i_long} = 0.174 S/m and σ_{i_trans} = 0.019 S/m. For the interstitial conductivities σ_{e_long} = 0.625 S/m and σ_{e_trans} = 0.236 S/m were taken. For case 2) σ_{e_trans} was set to 0.068 S/m to fit the requirement of equal anisotropy ratios. The bath conductivity σ_{bath} was 1.0 S/m.

Results

For all stimulation sites, AP propagation was initiated with varying myocardial parameter settings. Consistent with [7,8], for stimulation at site C the shape of the depolarization wavefront was either a sphere (isotropic case), a prolate spheroid (anisotropic case), or a twisted prolate spheroid (anisotropic case with transmural fiber rotation). In Figure 4A, I_m wavefronts for these three cases are shown. During depolarization differences in Φ_e due to AP shape heterogeneity were not observed. The wavefronts corresponding to settings 5 and 6 were similar to the homogeneous settings 3 and 4.

In the isotropic case, the conduction velocity was 0.3 m/s, whereas with anisotropy 0.5 m/s and 0.15 m/s were observed in the longitudinal and transversal direction, respectively.

ISSN: 1727-1983

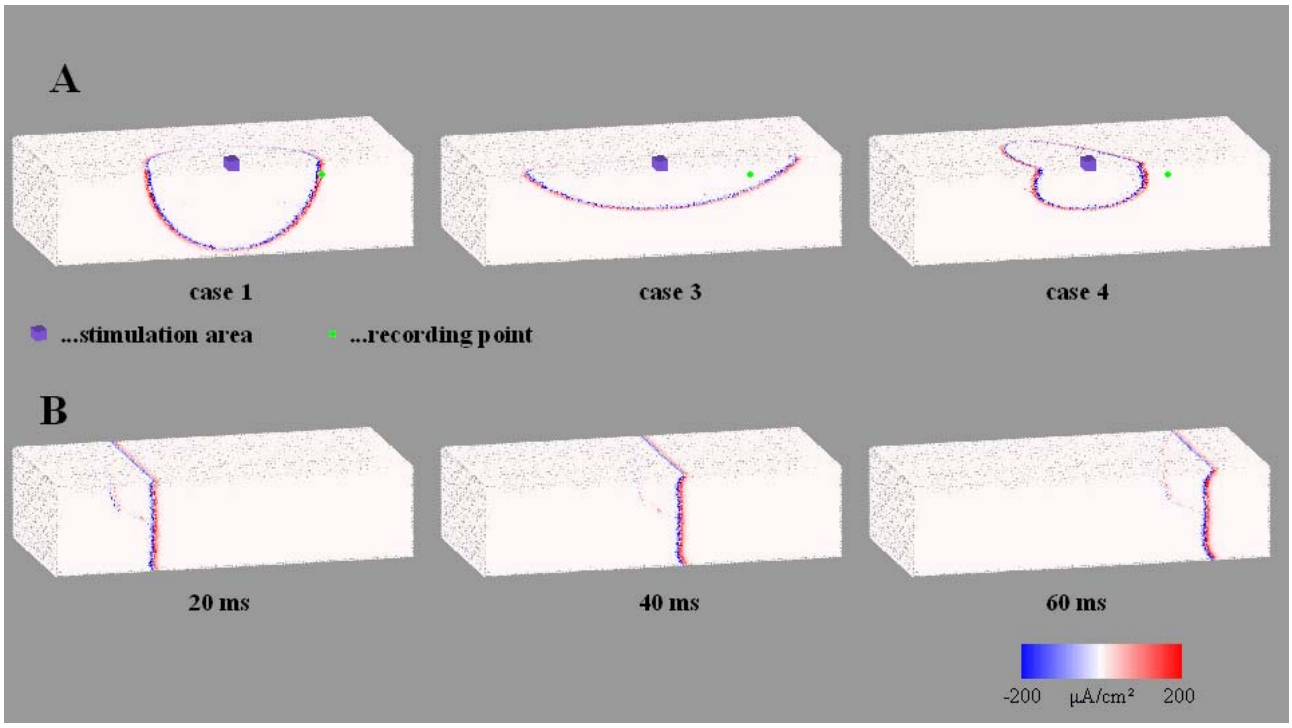

Figure 4: A) Wavefront pattern of the transmembrane current for different settings (isotropic case, anisotropic case and anisotropic case with fiber curvature) 30 ms after stimulation at site C (Figure 1). For a better insight the slab is halved. The observation point for the potentials presented in Figure 5 is marked. B) Propagation of a planar depolarization wave along the longitudinal direction for case 3, with increasing bending of the front due to the increased load near the surface (electrotonic effect).

For planar wavefronts, an increased bending of the wavefront during propagation through the myocardium is clearly visible due to a higher load near the epi- and endocardial surfaces (Figure 4B).

Figure 5 shows Φ_e for different parameter settings. The location of the observation site is marked in Figure 4A (in 1 cm distance to the stimulation area 1 mm beneath the epicardial surface). All signals Φ_e at this location are of biphasic shape corresponding to the passage of the depolarization wavefront. However, distinct differences are visible due to different conductivity settings and fiber orientation which gave rise to differently shaped wavefronts.

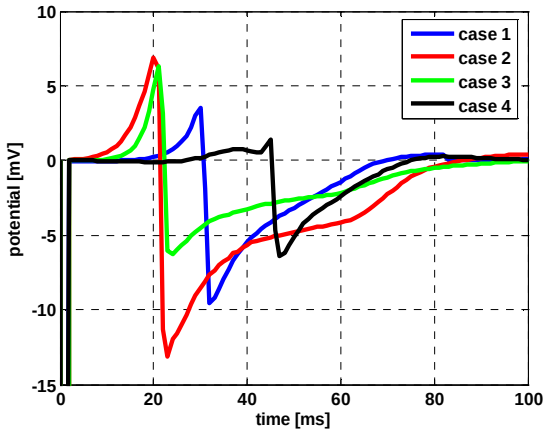

Figure 5: Extracellular potentials Φ_e during depolarization for cases 1-4. Recording point marked in Figure 4A.

For case 2, the amplitude of the Φ_e inside the myocardium is clearly higher as compared with case 3. This finding is due to the significantly reduced conductivity in the extracellular space for the case with equal anisotropy.

Especially for measurement points near the stimulation area from where the depolarization wave takes longer until encountering any border, the effect of the disappearance of the front is explicitly visible as a decline in the Φ_e shape, for example, the distinct reduction of Φ_e in Figure 5 for the cases 2 and 3 at 40 ms when the endocardial border is reached.

In the case with fiber rotation the volume of the depolarized region grows significantly faster than for the case with straight parallel fibers (Figure 6).

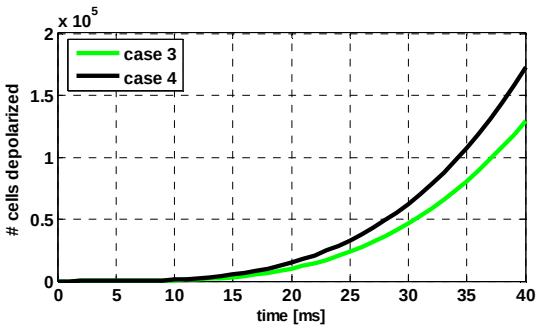

Figure 6: Number of cells depolarized after stimulation on site C with (case 4) and without (case 3) fiber rotation.

ISSN: 1727-1983

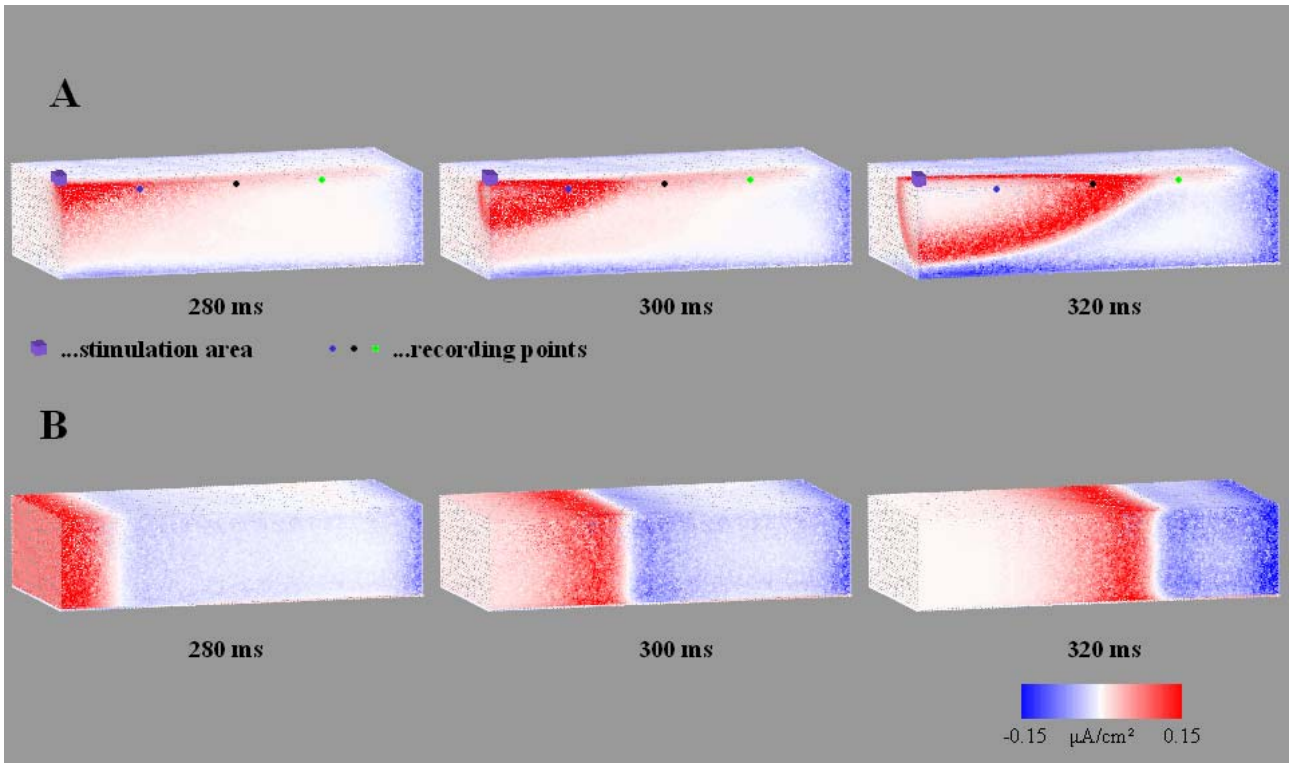

Figure 7: A) Distribution of the transmembrane current during repolarization phase for a case 3 setting with stimulation on position L (Figure 1). The slab is halved again and the blurred repolarization wave is visible. The recording points for the potentials presented in Figure 8 and 9 are marked. B) Repolarization process for a planar stimulation of the entire left surface. The parameter setting was case 3.

Unlike depolarization, the repolarization process has no typical narrow wave characteristic. However, it can be understood as a proceeding wave phenomenon. Surrounding the stimulation area, a region with positive I_m is built up. Therefore in this localization the resulting extracellular potential is positive only. In distance to the stimulation site the repolarization phase forms its wave-like appearance (Figure 7). There the interstitial potential shows a biphasic shape with a polarity opposite to that during depolarization. Figure 8 illustrates the computed potentials for the three marked positions in Figure 7A.

Human ventricular myocardium has no uniform AP distribution. For case 5 and case 6 the heterogeneity of the AP was approximated by three layers (Figure 3A) with different AP shapes. The repolarization phase of the APs is now temporally desynchronized. The resulting extracellular potentials for these cases during repolarization are therefore shifted and the maximum amplitude is reduced (Figure 8).

An important AP parameter is the basic cycle length (BCL). A reduction of the BCL reduces the APD leading to a shortening of the calculated potentials.

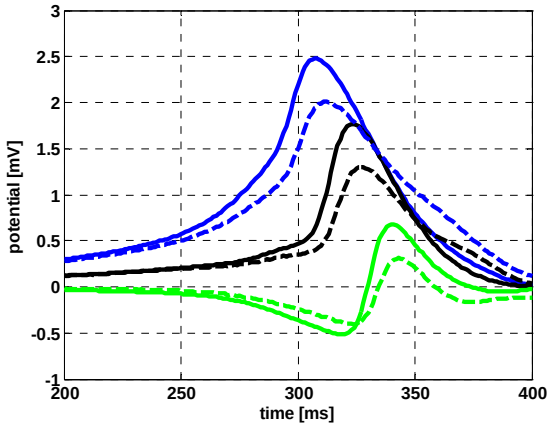

Figure 8: Extracellular potentials Φ_e during repolarization for the three observation points marked in Figure 7A with (dashed) and without (solid) transmural AP heterogeneity.

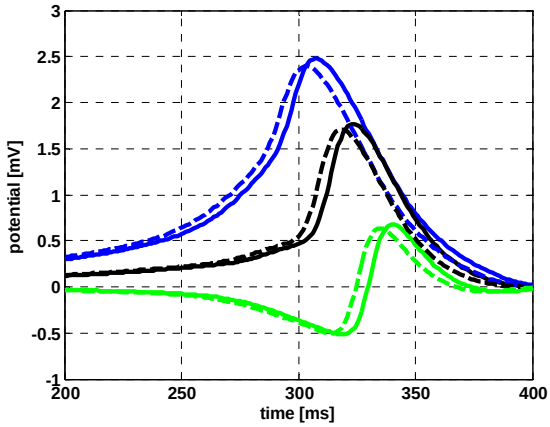

Figure 9: Extracellular potentials Φ_e during repolarization for the three observation points marked in Figure 7A for case 3 with BCL = 1000 ms (solid) and BCL = 600 ms (dashed).

ISSN: 1727-1983

This effect is clearly visible during repolarization. To simulate the effect of a higher heart rate first a single cell was excited for a hundred times with the chosen BCL to obtain the kinetic model parameters at the moment just before the next stimulus would have been applied. Then the whole slab model was initiated with the calculated parameter values. In Figure 9 the results of a reduction of the BCL can be seen for the positions marked in Figure 7A.

The signal characteristic of a positive epicardial potential during repolarization near the stimulation area and wave-like behaviour in the distance could also be observed in recorded signals from a pacemaker patient with epicardial electrodes (Figure 10). The recording electrode was placed near the left ventricular apex. For signal AA the sensing electrode is also used for pacing. For potential VA the pacing electrode is positioned at the right ventricular outflow tract approximately 6 cm apart from the recording electrode. No recording was possible during the blanking period of 32 ms subsequent to the pacing impulse.

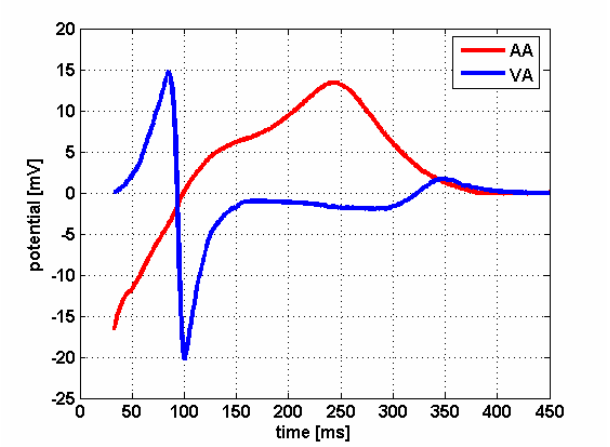

Figure 10: Recorded epicardial potentials from a pacemaker patient. AA… pacing and sensing electrode in same position, VA… electrodes apart.

Discussion

A slab model was presented which is capable of simulating the electrical activity of cardiac tissue with fiber rotation and transmural heterogeneities. With this model the influences of different parameter settings and different tissue specifications can be demonstrated. The accurate determination of the tissue parameters is a challenging problem because the values in literature show a large variation. For our setup the conductivity parameters are based on data from Clerk [9].

An entire AP cycle was simulated and therefore expands further studies [7,8], which concentrated on stimulation and depolarization. Results regarding the stimulation and exciation spreading as well as the influence of the fiber rotation are comparable for both studies.

Studies with focus on the repolarization phase [10,11] simulate the influence of different AP shapes on the surface ECG (far field) however not on epimyocardial electrograms (near field). The simulated morphological pattern of the Φ_e during the repolarization period are in accordance with recorded signals from pacemaker patients.

Especially for the interpretation of recorded signals the anatomical details and the physiological state of the analyzed heart have to be known very well. Therefore a kinetic model based on human ventricular data [6] was used for simulation of the AP shapes. Human ventricular myocardium will not have such distinct layers with different AP shapes like those used for the presented simulations, i.e. the AP variation can be assumed to change more smoothly. However in the described model the effect how AP variations alter Φ_e can be studied.

Until now the recording electrodes are simulated as point-like electrodes. A more realistic approach would be a passive metal area with high conductivity surrounded by an also passive tissue region with low conductivity to mimic the fibrotic capsule covering the electrode after implantation.

For the simulation with reduced BCL, the kinetic model in the whole slab was initialized with the same state vector. This small slab geometry has propagation times with some ten ms, therefore this assumption has only a minor impact. For whole heart simulations a gradually different setting along the excitation spreading has to be considered.

Conclusions

Model-based interpretation of epicardial electrograms is the only chance to utilize the diagnostic potential of these signals. Therefore the simple slab model will be further refined by first modeling a human wedge preparation based on CT geometry data, and finally, the whole human ventricles to be able to compare simulation results with available human epicardial recordings. Further clinical studies and model-based investigations are required for a more complete validation. These efforts are justified by the already obtained results.

Acknowledgement

Research was supported by the Austrian National Science Foundation FWF under grant P 16965. The measured data was taken from the CHARM Database (by courtesy of CORTRONIK, Graz).

References

[1] AUER T., SCHREIER G., HUTTEN H., et al. (1996): 'Paced epimyocardial rejection monitoring after heart transplantation', *J Heart Lung Transplant*, **15(10)**, pp. 993-8

[2] HUTTEN H., KASTNER P., SCHREIER G., et al. (1998): 'Hemodynamic assessment by evaluation of intramyocardial electrograms', Proc. 20th Ann. Int. Conf. IEEE-EMBS, Hongkong, 1998, pp. 395-8

ISSN: 1727-1983

[3] EBNER E., KRATSCHMER H., DANILOVIC D., et al. (2004): 'Ventricular evoked response as clinical marker for hemodynamic changes in dilative cardiomyopathy', *Pacing Clin Electrophysiol.*, **27(2)**, pp. 166-74

[4] VIGMOND E.J., AGUEL F., TRAYANOVA N.A. (2002): 'Computational Techniques for Solving the Bidomain Equations in Three Dimensions', *IEEE Trans. Biomed. Eng*., **49(11)**, pp. 1260-9

[5] WEBER DOS SANTOS R., PLANK G., BAUER S., VIGMOND E.J. (2004): 'Parallel multigrid preconditioner for the cardiac bidomain model', *IEEE Trans. Biomed. Eng.*, **51(11),** pp. 1960-8

[6] TEN TUSSCHER K.H.W.J., NOBLE D., NOBLE P.J. AND PANFILOV A.V. (2004): 'A model for human ventricular tissue', *Am J Physiol*., **286(4)**, pp. H1573-89

[7] MUZIKANT A.L., HENRIQUEZ C.S. (1998): 'Bipolar Stimulation of a Three-Dimensional Bidomain Incorporating Rotational Anisotropy', *IEEE Trans. Biomed. Eng.*, **45(4)**, pp. 449-62

[8] HENRIQUEZ C.S., MUZIKANT A.L., SMOAK C.K. (1996): 'Anisotropy, fiber curvature and bath loading effects on activation in thin and thick cardiac tissue preparations: Simulations in a three-dimensional bidomain model', *J. Cardiovas. Electrophysiol.*, **7(5)**, pp. 424-45

[9] CLERK L. (1976): 'Directional differences of impulse spread in trabecular muscle from mammalian heart', *J Physiol.*, **255(2)**, pp. 335-46

[10] VAN OOSTEROM A. (2001): 'Genesis of the T wave as based on an equivalent surface source model', *J Electrocardiol*., **34(Suppl)**, pp. 217-27

[11] TYŠLER M., TURZOVÁ M., ŠVEHLIKVÁ (2003): 'Modeling of heart repolarization using realistic action potentials', *Measurement Science Review*, **3(2)**, pp. 37-40

ISSN: 1727-1983